筑　波　大　学

博 士 （医 学） 学 位 論 文

Pathophysiology of "upstream" pulmonary veins in pulmonary vein stenosis; with emphasis on the potential role of endothelial-mesenchymal transition

(肺静脈狭窄成立過程における endothelial-mesenchymal transition 現象の関与の可能性)

2017

筑波大学

加藤秀之

Table of Contents

[Abstract]

Objectives: Pulmonary vein stenosis is a rare disease with a dismal outcome. Surgical and catheter-based interventions on pulmonary veins are associated with recurrent pulmonary vein stenosis (PVS) which can progress diffusely through the 'upstream' pulmonary veins. Once it has diffuse progress, the malignant clinical course will follow without any effective treatment. The mechanism has been rarely studied. We used a porcine model of PVS to assess disease progression with emphasis on the potential role of endothelial-mesenchymal transition (EndMT).

Methods: One-week-old piglets underwent bilateral pulmonary vein banding in which all pulmonary veins have a band around them (Banded, n = 6). Staged operation was applied. A left thoracotomy was performed for the left side pulmonary vein banding, followed by the right side pulmonary vein bading via a right thoracotomy a week later. The bands tightened the pulmonary veins as the piglets grew. Sham operations mimiced the banding procedure without a band placed around pulmonary veins (Sham, n = 6). Additional piglets underwent identical banding procedure and stent implantation in a single banded right middle pulmonary vein three weeks post-banding (Stented, n = 6). Seven weeks post-banding, hemodynamics and upstream PV pathology were assessed focusing on EndMT marker expression.

Results: All Banded piglets developed significant pulmonary hypertension and RV hypertrophy 7 weeks after the banding. The upstream pulmonary veins exhibited intimal thickening associated with features of EndMT including: increased TGF-β1 and Smad expression, loss of endothelial and gain of mesenchymal marker expression. Furthermore, intimal cells from upstream pulmonary veins in the banded group demonstrated co-expression of endothelial and mesenchymal markers, which indicates that the EndMT process occurs in the upstream pulmonary veins under pulmonary vein stenosis. These immunopathological changes and a prominent myofibroblast phenotype in the remodeled pulmonary veins were

consistently identified in specimens from patients with PVS implying clinical relevance of the piglet PVS model. *In vitro* TGF-β1-stimulated cells isolated from piglet and human pulmonary veins, and human umbilical vein endothelial cells all acquired myofibroblast phenotype expression supporting the hypothesis in which TGF-β-mediated EndMT could occur in pulmonary venous endothelial cells. After stent implantation, although in-stent stenosis was developed aggressively in 4 weeks, temporary decompression of a pulmonary vein was associated with re-appearance of endothelial marker expression suggesting the potential for plasticity in the observed pathologic changes.

Conclusions: Neonatal pulmonary vein banding in piglets recapitulates critical aspects of clinical PVS and highlights a pathologic profile consistent with EndMT - supporting the rationale for evaluating therapeutic strategies designed to exploit reversibility of upstream pulmonary vein pathology.

[Introduction]

3.1 Clinical translation

Pulmonary vein stenosis (PVS) occurs as either a primary congenital or an acquired disease after repair of total anomalous pulmonary venous drainage (TAPVD) [1-3]. The outcomes associated with PVS are dismal irrespective of clinical context. Surgical and stent-based strategies to treat PVS necessarily involve some component of pulmonary vein injury and are associated with high rates of recurrent PVS and progression to end-stage disease [4]. When recurrent, surgical and catheter-based interventions can treat local PVS at the left atrial-pulmonary vein junction, however they cannot treat the upstream pulmonary venous disease which persists after treatment and dictates the likelihood of survival – with probability of survival of less than 20% at one year for patients with diffuse involvement of all four pulmonary veins [5, 6]. Repeat surgical interventions are often not feasible and, as a last resort, palliative stenting of the pulmonary veins is performed with re-stenosis rates of 46% at 6 months and 63% at one year – with patient survival of 66% at two years [7].

A unique characteristic of the clinical syndrome is the potential for progressive and diffuse stenosis throughout the pulmonary venous system. Although commonly manifest as a local stenosis at the pulmonary vein-left atrial junction, the most malignant form of the disease is characterized by diffuse involvement of the 'upstream' pulmonary veins extending into the lung parenchyma. Because of the diffuse nature of upstream pulmonary vein involvement, chemotherapy protocols have been undertaken to treat diffuse PVS – without success [8]. With the diffuse upstream lesion, PVS leads to relentless pulmonary hypertension, right heart failure, and death. Despite scattered recent reports of catheter-based interventions and surgical procedures [9, 10], the overall prognosis is poor [5-7, 11]. Remarkably, the cellular

mechanisms and pathophysiology that cause upstream PVS remain incompletely explored and, as a result, there is no known medical therapy that ameliorates diffuse PVS disease.

3.2 Endothelial cell injury triggers cellular phenotype transition

Recently, we have made an observation that cells isolated from specimens acquired during surgical repair of TAPVD exhibit loss of an endothelial cell layer and obtained proliferation of mesenchymal cellular phenotype cells including myofibroblasts (MyoFB). This process resembles endothelial-mesenchymal transition (EndMT), which appears to parallel the more commonly described epithelial-mesenchymal transition (EpiMT), and has been implicated in fibrogenic diseases and vascular remodeling [12].

3.3 Epithelial-mesenchymal transition (EpiMT)

EpiMT is a process in which cells lose their epithelial phenotype and acquire characteristic features of mesenchyme [13]. It is a highly orchestrated and regulated process, resulting in the loss of epithelial cell adhesion, disruption of tubular basement membrane, and enhanced cell migration and invasion [13]. The critical molecular hallmarks of EpiMT include repression of E-cadherin, acquisition of a migration-competent, spindle cell phenotype with expression of fibroblastic specific protein 1 (FSP-1), and the production of extra-cellular matrix comprised principally of collagen I and fibronectin [14]. Three types of EpiMT are known; Type 1 EpiMT involves primitive epithelial cells transitioning to motile mesenchymal cells as part of gastrulation and during cardiac valve formation [15]. Type 2 EpiMT involves secondary epithelial or endothelial transitioning to resident tissue fibroblasts, and can occur in somatic organs such as lung, heart, and kidney as an inducible fibrogenic response consequent to persistent inflammation [15]. Type 3 EpiMT is epithelial cell transitioning to mesenchymal phenotype seen in the metastasis process of the cancer [15].

3.4 Endothelial-mesenchymal transition (EndMT)

EndMT refers to the analogous process through which endothelial cells lose endothelial characteristics and gain expression of mesenchymal, myofibroblast-like characteristics [12]. Although less frequently investigated than EpiMT, EndMT is known to occur during normal cardiac and vascular development as well as during pathophysiological vascular remodeling [15]. EndMT refers to a process whereby endothelial cells respond to an injury stimulus (e.g. increased wall stress) by losing endothelial cell markers (e.g. E-Cadherin, CD-31), and gaining expression of mesenchymal myofibroblast markers (e.g. α-smooth muscle actin (α-SMA), FSP-1). During this process, the endothelial cells lose polarity and cell-cell contacts, acquire an invasive migratory phenotype, and transition into a spindle shape [12]. Importantly, plasticity between EndMT and the reverse process (mesenchymal-endothelial transition), is dynamic and can be pushed in either direction, suggesting potential for the reversibility of the pathologic changes for an undefined period of time after initiation [15]. We propose that the fibrogenic response seen in PVS represents a pulmonary vein-specific form of EndMT.

3.5 TGF-β mediated pathological process

Transforming growth factor-β (TGF-β) is a known mediator of EndMT in pathologic processes and in normal cardiovascular development [12, 15-17]. Inhibition of TGF-β in pressure-overloaded rodent models of EndMT is sufficient to block myocardial fibrosis [15, 18]. Important mediators of TGF-β-induced EndMT include Smad3 and Snail [15]. TGF-β levels are increased in the pulmonary vasculature of rats with pulmonary hypertension and TGF-β superfamily signaling has been identified as a trigger of pulmonary arterial hypertension [19, 20]. The role of TGF-β in pulmonary venous hypertension has been rarely described with

only two isolated reports describing increased levels of TGF-β after pulmonary venous injury induced by radiofrequency ablation of adult pulmonary veins [21, 22].

3.6 Study objectives

In order to investigate the cellular mechanisms associated with PVS, we utilized a neonatal piglet model which was previously established by LaBourene et al [23] and recapitulates the clinical and pathological PVS with the objective of examining the histopathology of upstream PVS to characterize the diffuse fibrogenic response in the pulmonary veins, hypothesizing EndMT-like phenotype change is attributed to the disease process. Furthermore, we investigate whether pathological reversibility or regression at the cellular level is witnessed in the upstream pulmonary veins after treating the PVS with stent deployment.

3.7 Hypothesis

We hypothesize that obstructed pulmonary veins undergo endothelial cell injury and trigger TGF-β mediated EndMT-like transformation of their endothelial cell layer as a critical early stage in the pathogenesis of PVS – which ultimately leads to progressive fibrogenesis characteristic of PV occlusive disease, producing a pathologic cellular phenotype that includes loss of endothelial cell properties and gain of MyoFB properties (Figure 1). Blocking the conversion of endothelial cells to this pathologic cell type, or stent-based reduction in pulmonary venous obstruction may reverse the upstream pulmonary venous disease progression.

[Methods]

4.1 Research ethics board approval

The Animal Care Committee at the Hospital for Sick Children approved the animal studies in accordance with the Terms of Reference following the Canadian Council on Animal Care Guidelines and federal/provincial legislations. Human samples were acquired with approval of the Research Ethics Board protocols under the auspices of the Heart Centre Biobank Registry (#1000011232, #0020010432).

4.2 Piglet pulmonary vein stenosis model

One-week-old Yorkshire piglets (3.9 ± 0.8 kg) underwent staged bilateral pulmonary vein banding (Banded, n = 6) or sham operations (Sham, n = 6). After anesthesia and intubation, piglets underwent staged operations as previously described [23]. Piglets were anesthetized with atropine, ketamine, and isoflurane, intubated and ventilated on a ventilator. General anesthesia was maintained with isoflurane (2-3 %), air (70 %), and oxygen (27 %) under positive pressure ventilation (20 cm H_2O, 30 - 40 breaths/min). Staged operations were adopted as previously described [23]. First, the individual banding of left pulmonary veins and common lower pulmonary vein was performed via a left 5th intercostal space thoracotomy. One week later, the individual banding of the right upper and middle pulmonary veins was carried out via a right 4th intercostal space thoracotomy. Bupivacaine (0.5 %) was injected for intercostal nerve blocks. A 1/8 inch-wide cotton umbilical tape was fixed around the pulmmonary vein with a length equivalent to 1.3 times the pulmonary vein circumference. 5 % dextrose lactated Ringer's solution (150 ~ 175 cc), cefazolin (40 mg/kg iv) and procaine penicillin G (30,000 units/kg im) were administered. Bupremorphine (0.02 mg/kg, every 8 hours, 3 days, im) and Meloxicam (0.4 mg/kg, every 24 hours, 3 days, p.o.) were given for pain

control. Sham-operated piglets underwent identical banding procedures but the band was not left in place.

Echocardiography was performed under anesthesia with ketamine and isoflurane before banding/sham operation and at 3 and 6 weeks post-procedure. At 7 weeks after bilateral banding/sham procedures, the piglets were anesthetised and instrumented to monitor hemodynamic parameters using 5 Fr thermodilution catheters (Teleflex, Limerick, PA). Systemic blood pressure (SBP), pulmonary arterial pressure (PAP), pulmonary capillary wedge pressure (PCWP), right ventricular pressure (RVP), and central venous pressure (CVP). Cardiac output (CO), pulmonary vascular resistance: (mean PAP – PCWP) / CO), systemic vascular resistance (SVR: (mean SBP – CVP) / CO), and compliance of the pulmonary artery (Comp: 1000 × CO / (mean PAP – PCWP)) were measured. Cardiac output was determined by injection of 23 ± 1 C˚saline (5 cc) into main PA and calculated with cardiac output computer (Model 9520A, Edwards Lifesciences, Irvine CA). Subsequently, a median sternotomy was performed and left and right ventricular pressures were measured simultaneously by apical catheterization. Lung biopsies were taken from each left distal middle lobe. The heart and lungs were quickly removed en bloc and dissected on a bed of ice. The upstream pulmonary veins were obtained, excluding pulmonary veins within the first 10 mm from banded sites, and sectioned for the primary cell culture, fixed in 10 % formalin, or frozen. Hematoxylin and eosin (HE) staining was used to show the intimal thickness and pulmonary vein morphology. Intimal thickness was assessed by measurement of the ratio of intimal to intimal + medial layer thickness at eight radial points in each pulmonary vein.

4.3 Stent implantation

Other six piglets were allotted for stent treatment (Stented, n = 6). Three weeks after identical bilateral pulmonary vein banding with the banded group, the stented group underwent

placement of bare-metal stents (Driver, Medtronic Inc., Minneapolis, MN) into the right middle pulmonary vein via femoral vein catheterization with 8Fr sheaths under fluoroscopic and intracardiac echocardiographic guidance (8 Fr AcuNav catheter, Biosense Webster, Diamond Bar, CA). After atrial septum puncture with a pediatric transseptal needle (COOK, Bloomington, IN), using a 6F RunWay WRP guide catheter (Boston Scientific Corp., Natick, MA), a bare-metal stent (3.5 or 4.0 mm in diameter) was deployed into the banding site of right middle pulmonary vein. Acetylsalicylic acid 10 mg/kg/day (Tanta pharmaceuticals Inc., ON, Canada) and clopidogrel 2.5 mg/kg/day (Teva Canada, ON, Canada) were given orally until the end point of the study. Seven weeks post-banding, invasive hemodynamics were measured and tissues were excised as described above. The stented portions of the pulmonary veins were excised and cross-sectioned at 3 points within the stent (proximal, middle and distal) cut by an Isomet slow-speed saw (Buehler, Lake Bluff, IL) and tungsten carbide knife. The percentage of in-stent re-stenosis was quantified using Image J software (National Institutes of Health, Bethesda, MD) according to the following formula: 100 × (ICM-LA) / ICM (ICM = inner area of the internal circumference of the media, LA = inner area of internal circumference of the intima) [24-26].

4.4 Human tissue

Pulmonary vein specimens were obtained from three patients with PVS. One patient had recurrent PVS after TAPVD repair (at two days of age) followed by reoperation for progressive PVS (at three months of age) and subsequent death. Autopsy specimens were stained for immunofluorescence as described below (Figure 2C-G). A second patient, with a diagnosis of tetralogy of Fallot and PVS, underwent intracardiac repair and pulmonary vein stent implantation at the age of 17 months. However, subsequent in-stent re-stenosis and severe pulmonary hypertension resulted in death at age 20 months. At autopsy, Movat pentachrome

staining was performed to assess the PV morphology in one patient (Figure 2A). A third patient, diagnosed with hypoplastic left heart syndrome, had recurrent refractory PVS after heart transplant at the age of five months and died at the age of nine months. Elastic Masson's trichrome staining of the pulmonary veins was employed at autopsy (Figure 2B).

Control human pulmonary vein tissues were obtained from a heart transplant donor who was two months old and did not have pulmonary vascular disease, which were analysed using the same immunofluorescence protocols (Figure 2H-L) and cultured for High-Content Imaging (HCI) analysis.

4.5 RV cellular size, myocardial fibrosis and collagen deposition

Transmural blocks of the right ventricular myocardium from banded and sham groups were fixed in 10% formalin and sectioned and stained with HE and Masson's trichrome stains [27]. All the slides were stained at the same time under identical conditions. The RV free walls were separated into three areas (Epicardium, myocardium and endocardium). Myocardial section was examined by 40 X objective lens and 10 X eyepiece. Total 60 randomly selected high power fields (HPF, 400 X) per piglet were used for analysis of cellular size and cardiac fibrosis. The diameters of cells from each area were determined by measuring the distance across the cell at its narrowest plane across the nucleus (Image J). The area of myocardial collagen content for each high power field slide was quantified (Photoshop CS4) and the area of blue stain was expressed as a percentage of the entire slide. The mean of these measurements from three RV layers was calculated.

4.6 Immunofluorescence

Paraffin-embedded tissue slides were deparaffinized in xylene and rehydrated in ethanol. Antigens were remasked with Sodium Citrate Buffer (Dako, Glostrup, Denmark), then

immersed in blocking buffer for 40 minutes and incubated with primary antibodies CD31 (1:100, Abcam, Cambridge, UK), fibronectin (1:200, BD Transduction Laboratories, Franklin Lakes, NJ), vascular endothelial-cadherin (VE-cadherin, 1:100, Thermo Fisher Scientific, Waltham, MA), alpha-smooth muscle actin (α-SMA, 1:100, Santa Cruz Biotechnology), fibroblastic specific protein 1 (FSP-1)/S100A4 (1:100, Millipore), von Willebrand factor VIII (vWF, 1:100, Dako) and TGF-β1 (1:100, Abcam) for 2 hours at room temperature, followed by the secondary anti-rabbit antibody (1:1000) and anti-mouse FITC (1:100) for 1 hour at room temperature. Slides were visualized using Quorum WaveFX-X1 Spinning Disc Confocal System (Quorum Technologies, ON, Canada) and Volocity software (PerkinElmer Inc., Waltham, MA).

4.7 Protein extraction and western-blot analysis

Upstream PV samples from piglets were homogenized in lysis buffer, centrifuged for 20 min at 13,400 g at 4°C and the supernatants were collected. Protein extracts were quantified with Bradford protein assay (Bio-Rad, Hercules, CA). Samples were separated on 10 % polyacrylamide gels, transferred to nitrocellulose membranes, and blocked with 5 % skimmed milk for one hour. The membranes were probed with CD31 (1:1000), VE-cadherin (1:1000), α-SMA (1:1000), TGF-β1 (1:1000), Smad4 (1:500, Abcam) and GAPDH (1:6000, Sigma-Aldrich, St. Louis, MO). Blots were then incubated with goat anti-mouse IgG-HRP (1:10,000) and goat anti-rabbit IgG-HRP (1:5000) secondary antibodies. Membranes were developed with ECL substrate (Santa Cruz Biotechnology). Densitometry was analyzed using Quantity One and Image Lab analysis software (Bio Rad Laboratories, Hercules, CA). GAPDH was used to verify all protein loads and normalize data.

4.8 Isolation and cell culture

Pulmonary vein samples from piglets and human were minced and washed with phosphate-buffered saline (PBS). Cell isolation was performed with 5% trypsin and 1 mg/ml type II collagenase in 20% glucose PBS at 37°C (pH 7.4). After isolation, the cells were cultured in Iscove's modified Dulbecco medium (Life Technologies, Carlsbad, CA) with antibiotics and incubated in 5 % CO_2 at 37 °C. Human umbilical vein endothelial cells (HUVEC) were purchased from ATCC (Manassas, VA) and cultured in the same manner.

Cultured human PV cells from a heart transplant donor, banded piglet PV cells, and HUVECs were treated with 5ng/ml recombinant human Transforming Growth Factor-Beta1 (TGF-β1) (R&D systems Inc., Minneapolis, MN) for 48 hours to mimic the EndMT process [12]. Cells that were not treated with TGF-β1 served as controls. 96- or 384-well plates were used to grow, stain, image and analyze cells in a semi-automated fashion using High-Content Imaging to increase reliability and statistical significance. Immunofluorescence was performed using the fibronectin (1:100) and α-SMA (1:100) antibodies. Nuclei were stained with Hoechst (1x). Samples were imaged in a Cellomics VTI automated high-content imager and analysed using a combination of Image J and custom written software. Integrated fluorescent intensity per cell were counted. For all three cell types, more than 400 cells per condition were tested, in triplicates.

4.9 Statistical analysis

Continuous variables were expressed as mean ± standard error of the mean. The unpaired *t* test was used for comparisons in echocardiography data, western-blot analysis data, and intimal thickness data between banded and sham groups. Multiple group comparisons between sham, banded, and stented groups were compared by one-way ANOVA followed by Tukey's post hoc test. HCI statistics were generated using custom scripts written for the R

software package and represented as Winsorized means (5 % tails) and p-values were calculated by Mann-Whitney test.

[Results]

5.1 Human PVS induces a decrease in endothelial and gain of mesenchymal markers in the hyperplastic intima

Histology staining in PV tissues from patients with progressive PVS demonstrated fibromuscular hyperplasia in the intima of the pulmonary veins (Figure 2A) and arterialization of a pulmonary vein with marked luminal narrowing (Figure 2B). In the patient with obstructed TAPVD, Immunofluorescence showed that the pulmonary veins had greater expression of fibronectin and α-SMA, diminished expression of CD31 and vWF, and exhibited stronger TGF-β1 expression compared with control human pulmonary veins (Figure 2C-L). The loss of endothelial markers and gain of mesenchymal markers indicated a possible phenotypic conversion of the endothelium into reparative myofibroblasts, consistent with EndMT process.

5.2 Banding of the pulmonary veins reproduces functional consequences of human PVS in a porcine model

Echocardiography data in sham and banded groups were taken at 3 and 6 weeks after operation (n = 6 in each group). Pressure gradient over pulmonary vein in banded group elevates significantly at the 3 weeks after banding while right ventricular pressure demonstrates mild elevation. Six weeks post-banding, echocardiography demonstrated the pulmonary vein gradient increased progressively to 11.50 ± 4.76 mmHg (vs. 3.40 ± 3.36 mmHg in the sham group, $p < 0.01$) and accordingly elevated RV systolic pressure in the banded group (52.17 ±

18.03 mmHg vs 23.25 ± 3.30 mmHg in the sham group). There are no significant differences in other parameters (Table 1).

Consistent with PVS in human patients, banding of porcine pulmonary veins induced changes in hemodynamics. At seven weeks post-procedure, banded piglets had equivalent central venous pressure (4.83 ± 4.08 vs. 1.83 ± 1.47 mmHg), higher pulmonary capillary wedge pressure (11.33 ± 3.07 vs. 5.33 ± 2.14 mmHg, $p = 0.01$), systolic right ventricular pressure (38.8 ± 8.77 vs. 19.50 ± 2.43 mmHg, $p < 0.01$), and mean pulmonary arterial pressure (34.3 ± 8.89 vs. 12.0 ± 2.37 mmHg, $p < 0.01$) compared with sham animals. The ratio of mean pulmonary arterial pressure to mean systemic blood pressure was higher in banded piglets than in sham piglets (0.65 ± 0.18 vs. 0.23 ± 0.02 mmHg, $p < 0.01$). Cardiac output was not different between groups (0.14 ± 0.02 vs. 0.15 ± 0.02 L/min/kg, $p = 0.25$). Banded piglets had higher pulmonary vascular resistance (7.54 ± 2.91 vs. 1.44 ± 0.24 mmHg/l/min, $p < 0.01$), and lower pulmonary vascular compliance (1.81 ± 1.34 vs. 7.20 ± 1.57 ml/mmHg, $p < 0.01$) (Table 2).

Banded piglets had more RV hypertrophy compared to sham animals as assessed by the ratio of right ventricular weight to left ventricular plus ventricular septal weight (RV / LV + septum: 0.65 ± 0.10 vs. 0.35 ± 0.02, $p = 0.01$). Histological and morphological analysis demonstrated RV hypertrophy manifested with a greater average diameter of RV myocytes in the banded group (16.67 ± 1.12 vs. 13.95 ± 1.80 μm, $P = 0.02$) and a higher percentage of collagen deposition in the RV of the banded group compared with the sham group (7.96 ± 2.66 vs. 2.88 ± 1.02 %, $p = 0.01$) (Figure 3).

Stent implantation in a single pulmonary vein at three weeks after banding did not improve overall hemodynamics. There were no significant differences in any hemodynamic parameters when comparing stented and non-stented banded piglets seven weeks post-banding. (Central venous pressure; 4.83 ± 4.08 vs. 5.50 ± 2.88 mmHg, $p = 0.58$, pulmonary capillary wedge pressure; 11.33 ± 3.07 vs. 14.67 ± 3.67 mmHg, $p = 0.12$, systolic right ventricular

pressure; 38.8 ± 8.77 vs. 44.67 ± 9.69 mmHg, p = 0.30, mean pulmonary arterial pressure; 34.3 ± 8.89 vs. 37.7 ± 7.31 mmHg, p = 0.49, the ratio of mean pulmonary arterial pressure to mean systemic blood pressure; 0.65 ± 0.18 vs. 0.79 ± 0.15 mmHg p = 0.17, cardiac output index; 0.14 ± 0.02 vs. 0.14 ± 0.03 L/min/kg, p = 0.78, pulmonary vascular resistance; 7.54 ± 2.91 vs. 7.64 ± 2.58 mmHg/l/min, p = 0.61, and pulmonary vascular compliance; 1.81 ± 1.34 vs. 1.26 ± 0.53 ml/mmHg, p = 0.38, between the banded and stented group). The ratio of right ventricular weight to left ventricular plus ventricular septal weight did not differ between the banded and stented group. (RV / LV + septum: 0.65 ± 0.10 vs. 0.73 ± 0.15, p = 0.17) (Table 2).

5.3 Banding of porcine pulmonary veins mimics the intimal morphological changes observed in human PVS

Morphological changes in upstream pulmonary veins from the banded piglets were analyzed. These veins had greater intimal thickness compared to sham piglets (15.48 ± 8.76 vs. 3.07 ± 1.04 %, p < 0.01) (Figure 2M-P). Small pulmonary veins in the distal lung parenchyma had greater intimal hyperplasia and luminal stenosis compared to sham piglets (Figure 2Q-R). Next, we assessed fibroproliferative changes in upstream banded pulmonary veins by immunofluorescence and Western blotting. Compared to sham piglets, the upstream pulmonary veins in banded piglets had greater expression of the mesenchymal markers fibronectin and FSP-1, and myofibroblast marker α-SMA (Figure 4A-F). Western-blot analysis confirmed greater expression of α-SMA in upstream banded pulmonary veins compared to sham piglets (α-SMA / GAPDH; 1.03 ± 0.26 vs. 1.38 ± 0.26, p-value = 0.028, Figure 4).

To test whether fibroproliferative changes affected distribution and expression of endothelial markers, we immunostained for CD31, vWF, and VE-cadherin. Expression of all endothelial markers decreased in upstream banded pulmonary veins (Figure 4G-L), similar to

the changes seen in human PVS samples (Figure 2C-L). Western blotting confirmed lower expression of the endothelial markers CD31 and VE-cadherin in banded piglet pulmonary veins (CD31 / GAPDH; 0.20 ± 0.08 vs. 0.10 ± 0.07, p = 0.031 and VE-cadherin / GAPDH; 2.42 ± 0.58 vs. 1.72 ± 0.36, p = 0.017) (Figure 4). Double immunostaining of CD31 and α-SMA (Figure 5A-F) was performed to investigate the pathologic process associated with transition of individual cells with co-expression of endothelial and mesenchymal markers. Imaging revealed intermittent intimal cells co-expressing endothelial and mesenchymal markers in banded pulmonary vein cells (transitional cell phenotype) (Figure 5G). Co-expression of these markers was never observed in pulmonary veins of sham animals.

5.4 Intimal hyperplasia following pulmonary vein banding is associated with pro-fibrotic signalling events

One of major drivers of EndMT is TGF-β-mediated signalling events that involve phosphorylation and subsequent nuclear translocation of Smad [28, 29]. Expression of TGF-β1 in the pulmonary veins was greater in banded piglets compared to sham piglets (Figure 5H-I). Quantitatively, Western-blot analysis demonstrated increased expression of TGF-β1 and Smad 4 in banded upstream PVs compared to sham PVs (TGF-β1 / GAPDH; 1.15 ± 0.32 vs. 1.73 ± 0.34, p = 0.01, Smad 4 / GAPDH; 0.50 ± 0.15 vs. 0.76 ± 0.24, p = 0.05 Figure 5).

5.5 Stent implantation partially reverses the changes induced by experimental PVS

Seven weeks after pulmonary vein banding (four weeks after stent implantation), upstream pulmonary veins in the stented piglets demonstrated greater expression of TGF-β1 in comparison to sham animals but less expression than banded animals (by subjective evaluation of immunofluorescence images), suggesting partial down regulation of TGF-β expression, and partial reappearance of CD31 and vWF (endothelial marker) expression with enhanced and

localized fibronectin and α-SMA (mesenchymal and myofibroblast markers) expression in the intima (Figure 6A-J), consistent with partial reversal or delayed progression of the immunohistochemical features of EndMT. A cell layer expressing endothelial markers in the stent group formed jagged notches rather than a smooth even layer implicating acquisition of invasive phenotype. In stent re-stenosis reduced the luminal diameter within the stent by 43 ± 28 % four weeks after stent implantation in the porcine model (Figure 6K).

5.6 Three types of cultured cells are prone to experimentally induced EndMT

All three cultured cell types (banded piglet PV cells, human control PV cells, and HUVECs) demonstrated increased expression of the myofibroblast markers fibronectin and α-SMA after TGF-β1 exposure (integrated fluorescent intensity per cell, fibronectin; piglet cells; 1008 ± 89 vs. 1044 ± 120 a.u., $p < 0.05$, human cells; 3918 ± 111 vs. 4836 ± 123 a.u., $p < 0.05$, HUVECs; 1418 ± 102 vs. 2160 ± 176 a.u., $p < 0.01$, α-SMA; piglet cells; 3679 ± 167 vs. 5935 ± 400 a.u., $p < 0.01$, HUVECs; 1882 ± 160 vs. 2072 ± 189 a.u., $p < 0.05$. Figure 7). The increase in the MyoFB markers for the human and piglet PV samples illustrates that stimulation with TGF-β1 are able to recapitulate the pathologic process observed in the clinical condition and our whole animal model. Similarly, the increase in fibronectin and α-SMA in the HUVEC cells shows that, on a cellular level, stimulation with TGF-β1 are able to emulate EndMT with pure endothelial cells. This is consistent with our histology data that shows the gain of MyoFB cell markers with pulmonary vein banding and localization of this process to the endothelial layer of the vein. After all, the increase in the myofibroblast markers suggests that stimulation with TGF-β1 recapitulates the pathologic process observed in the *in vivo* animal model.

[Discussion]

We previously investigated a piglet model of progressive PVS which revealed increased pulmonary vascular resistance and degradation of the internal elastic lamina of the pulmonary veins [23]. The precise molecular pathways leading to the pulmonary venous fibrogenic response, however, remain unknown. Our piglet model mimics the critical aspects of clinical PVS, including myocardial change, hemodynamic deterioration, and pathological manifest in the upstream pulmonary veins. Examination of upstream pulmonary veins implicates involvement of EndMT in the pathologic process demonstrating loss of endothelial marker expression and gain of mesenchymal marker expression in the intima. Other data suggesting a role for EndMT in the pathology include the finding of co-expression of endothelial and mesenchymal markers in the pulmonary vein intimal cells of banded piglets - albeit at low frequency. The presence of such co-expression has been cited as supportive evidence for the intermediate stage of EndMT [15, 30, 31].

TGF-β - mediated EndMT has been observed to participate in several other fibrogenic diseases where vascular remodelling is a critical component of the pathologic process [12, 15, 32, 33]. In the current study, increased TGF-β and Smad 4 expression were also noted in the obstructed PVs from piglets. TGF-β is a well-known mediator of EndMT during cardiovascular development [12, 15-17]. Increased gene expression of TGF-β isoforms is associated with myocardial fibrosis in mice with pressure overload induced by aortic banding [34] and inhibition of TGF-β signaling in pressure-overloaded animal models of EndMT is sufficient to block myocardial fibrosis [15, 18]. In rat models of pulmonary hypertension, TGF-β levels are increased in the pulmonary vasculature and TGF-β signalling is identified as a trigger of pulmonary arterial hypertension [19, 20]. Smad is a downstream mediator in the TGF-β

signaling pathways with Smad 4, a common mediator interacting with receptor regulated Smads which, in turn, is associated with EndMT [32, 35-37]. These data are consistent with a model in which regulated TGF-β signaling in the pulmonary vein endothelium, likely resulting from abnormal hemodynamic shear stress, promotes EndMT, leading to the generation and proliferation of synthetic myofibroblasts within the pulmonary vein wall.

Our animal model induced the development of progressively severe right ventricular hypertrophy and pulmonary hypertension consistent with the clinical course seen in patients with severe PVS. The pulmonary veins of the affected piglets exhibited increased TGF-β expression, loss of endothelial markers and gain of mesenchymal markers consistent with the findings in the human PV samples derived from patients with fatal PVS. Our *in vitro* studies demonstrated that TGF-β-treated cells (human, piglet PV cells, and HUVECs) exhibited a similar pattern of mesenchymal/myofibroblast marker expression (fibronectin and α-SMA) that was evident in the piglet PVS model and implicates that EndMT-like process occurs in the local endothelium. Taken together, these results suggest that this piglet PVS model is consistent with the clinical, pathological and cellular changes found in patients with end stage progressive PVS.

Whereas local inflammation at banding site may have a role in diffuse PVS, these data suggest that upstream pulmonary vein endothelial injury is associated with elaboration of TGF-β, Smad signalling events, and proliferation of myofibroblasts in the pulmonary vein wall. Local inflammation from the banding material does, however, represent a limitation of our model. We have attempted to mitigate this limitation by examining the pulmonary veins "upstream" pulmonary veins at locations which were 10 - 40 mm away from banding site. We believe this distance is beyond the range of local inflammation. Although difficult to precisely identify the geometric extent of the local inflammatory effect, the examined upstream areas appeared on gross inspection to be free of obvious induration. Furthermore, our histologic

examination was consistent with human samples in which there were no implanted foreign bodies to create PVS.

Although our data were consistent with a role for EndMT in the observed pulmonary venous pathology, other mechanisms alone or in combination with EndMT may account for the fibrogenic response in the upstream pulmonary veins. The increased number of myofibroblasts may be derived from proliferation of local resident mesenchymal cells [38] or originate from circulating progenitor cells [39].

Proliferation of resident fibroblasts

Local resident fibroblasts have been hypothesized to be the main source of myofibroblasts in wound healing and tissue repair [40, 41]. In addition, migration and proliferation of smooth muscle cells and fibroblasts/myofibroblasts have been observed in studies of local tissue injury [42, 43]. Traditionally, stimulation and proliferation of resident fibroblasts was thought to be the sole origin of fibroproliferative disease [44]. However, more recent evidence suggests that contributions to a vascular fibroproliferative response can be the consequence of other processes including circulating bone marrow derived fibroblasts and endothelial-to-mesenchymal transition (EndMT) [12, 15].

Bone marrow derived progenitor cells

Alternatively, circulating bone marrow-derived mesenchymal progenitor cells are known to play an important role in tissue remodelling and fibrosis [45] and may contribute to the observed pulmonary venous pathology. In a model of hypoxia-induced pulmonary hypertension, Frid et al. demonstrated that remodelling of the pulmonary arteries required recruitment of circulating mesenchymal precursors [46]. The role of bone marrow derived progenitor cells in PVS is not well defined. In a model of pressure-overload induced myocardial fibrosis, evaluation of the origin of active fibroblasts demonstrated that a minority was derived from bone marrow precursors (~15%) and the remainder was derived from EndMT [15].

Although bone marrow derived progenitor cells are likely to be involved to some extent in PVS, there is abundant evidence that EndMT can be demonstrated in ex-vivo models (e.g. without circulating bone marrow derived progenitor cells) [16]. *In vitro* PV cell stimulation with TGF-β in the current study also revealed increased myofibroblast marker expression which suggests myofibroblast proliferation can occur in the local endothelium.

Thus, the complexity of in vivo histopathologic processes is likely to involve multiple mechanisms and proliferation of resident fibroblasts and/or recruitment of circulating progenitor cells may make substantial contributions to the observed pulmonary vein pathology in our model. However, given the observed substantial evidence of EndMT markers and TGF beta signaling pathway markers, EndMT is considered to be the culprit in the pathogenesis of PVS.

The use of high-content imaging in the present study demonstrates that TGF-β induces a myofibroblast phenotype in human and piglet pulmonary veins and in HUVECs. We propose that this cell-based assay, suitable for high-throughput screening, emulates a critical element in the genesis of PVS and could be used to evaluate libraries of compounds for their capacity to inhibit this process. This would advance the objective of developing therapeutic agents designed to target TGF-β1-mediated transformation and the disease-relevant molecular pathways leading to PVS.

Very few studies have evaluated the effect of stent implantation in obstructed pulmonary veins and these studies tend to focus on in-stent re-stenosis rather than the histopathology of the upstream pulmonary veins. Indeed, we noted significant in-stent re-stenosis within four weeks of stent placement, which is consistent with the limited efficacy of stents to treat pediatric PVS [7]. Furukawa et al. evaluated the effectiveness of drug-eluting stents in pig pulmonary veins [26]. However, in their study the stents were deployed in unobstructed pulmonary veins. In contrast, our report is the first to evaluate the efficacy of

stents in a model of progressive PVS. Future studies to test the efficacy of stents may be more informative if performed in the setting of an experimental model of PVS. The piglet model is a 'high yield' model because there is ample opportunity to study mechanisms of upstream PVS, in-stent restenosis, and right ventricular failure due to pressure overload, although those are beyond the scope of the current study.

Despite the temporary reduction of obstruction, upstream pulmonary veins responded to stent implantation with jagged layer of cells expressing some return of endothelial markers, diminished TGF-β expression and enhanced mesenchymal markers suggesting the potential for plasticity in the observed pathophysiologic process. Reversal of EndMT is known to occur, i.e. mesenchymal-endothelial transition [47]. Stenting appears to have initiated some reversal of the process possibly due to temporary relief of local pulmonary venous hypertension. Rapid in-stent re-stenosis, however, likely limited the efficacy of the intervention. We need to study more time points after stent implantation to better characterize the alterations in pulmonary venous pathology associated with relief of obstruction. The origin of the cells expressing endothelial markers after stenting is unclear and these cells could arise from mesenchymal-endothelial transition, circulating endothelial progenitor cells [48, 49] or enhanced re-expression from native endothelial cells. Although the mechanism is unclear, the potential for reversibility of the pathologic process warrants further investigation to develop novel adjuvant therapies designed to promote reversal of the process in concert with local surgical and stent-based decompression of pulmonary vein stenosis.

[Conclusion]

The piglet pulmonary vein stenosis model described herein recapitulates critical aspects of clinical PVS, including the myocardial alterations, hemodynamic sequelae, and the

histopathologic features in the affected pulmonary veins. Examination of the cellular response in upstream pulmonary veins reveals upregulation of TGF-β expression, loss of endothelial markers and gain of mesenchymal markers among constituent lesional cells, implicating EndMT in the pathologic process. Evidence of reappearance of endothelial marker expression with enhanced and localized mesenchymal and myofibroblast markers in the upstream pulmonary veins after stenting suggests potential regression of the pathologic process and an element of reversibility at the cellular level highlighting new avenues of investigation.

[Acknowledgements]

We wish to thank Wei Hui from Heart Centre Echocardiography Laboratory for performing Echocardiography and appreciate the contribution of participating surgeons, Drs, Glen Van Arsdell, Osami Honjo and Edward Hickey.

[REFERENCES]

1. Humpl T, Reyes JT, Erickson S, Armano R, Holtby H, and Adatia I. *Sildenafil therapy for neonatal and childhood pulmonary hypertensive vascular disease.* Cardiology in the Young, 2010. **21**(02): p. 187-193.
2. Grosse-Wortmann L, Al-Otay A, Goo HW, Macqoman CK, Coles JG, Benson LN, Redington AN, and Yoo SJ. *Anatomical and functional evaluation of pulmonary veins in children by magnetic resonance imaging.* J Am Coll Cardiol, 2007. **49**(9): p. 993-1002.
3. Karamlou T, Gurofsky R, Al Sukhni E, Coles JG, Williams WG, Caldarone CA, Van Arsdell GS, and McCrindle BW. *Factors associated with mortality and reoperation in 377 children with total anomalous pulmonary venous connection.* Circulation, 2007. **115**(12): p. 1591-8.
4. Seale AN, Uemura H, Webber SA, Partridge J, Roughton M, Ho SY, McCarthy KP, Jones S, Shaughnessy L, Sunnegardh J, Hanseus K, and Berggren H. *Total anomalous pulmonary venous connection: morphology and outcome from an international population-based study.* Circulation, 2010. **122**(25): p. 2718-26.
5. Yun TJ, Coles JG, Konstantinov IE, Al-Radi OO, Wald RM, Guerra V, de Olivira NC, Van Arsdell GS, William WG, Smalhorn J, and Caldarone CA. *Conventional and sutureless techniques for management of the pulmonary veins: Evolution of indications from postrepair pulmonary vein stenosis to primary pulmonary vein anomalies.* J Thorac Cardiovasc Surg, 2005. **129**(1): p. 167-74.
6. Viola N, Alghamdi AA, Perrin DG, Wilson GJ, Coles JG, and Caldarone CA. *Primary pulmonary vein stenosis: The impact of sutureless repair on survival.* J Thorac Cardiovasc Surg, 2011. **142**(2): p. 344-50.

7. Balasubramanian S, Marshall AC, Gauvreau K, Peng LF, Nugent AW, Lock JE, and McElhinney DB. *Outcomes after stent implantation for the treatment of congenital and postoperative pulmonary vein stenosis in children.* Circ Cardiovasc Interv, 2012. **5**(1): p. 109-17.

8. Rehman M, Jemkins KJ, Juraszek AL, Connor JA, Gauvreau K, Muneeb M, Sena LM, Colan SD, Saia T, and Kieran MW. *A prospective phase II trial of vinblastine and methotrexate in multivessel intraluminal pulmonary vein stenosis in infants and children.* Congenit Heart Dis, 2011. **6**(6): p. 608-23.

9. Hickey EJ, and Caldarone CA. *Surgical management of post-repair pulmonary vein stenosis.* Semin Thorac Cardiovasc Surg Pediatr Card Surg Annu, 2011. **14**(1): p. 101-8.

10. Caldarone CA, Najm HK, Kadletz M, Smallhorn JF, Freedom RM, William WG, and Coles JG. *Surgical management of total anomalous pulmonary venous drainage: impact of coexisting cardiac anomalies.* Ann Thorac Surg, 1998. **66**(5): p. 1521-6.

11. Caldarone CA, Najm HK, Kadletz M, Smallhorn JF, Freedom RM, Williams WG, and Coles JG. *Relentless pulmonary vein stenosis after repair of total anomalous pulmonary venous drainage.* Ann Thorac Surg, 1998. **66**(5): p. 1514-20.

12. Arciniegas E, Frid MG, Douglas IS, and Stenmark KR. *Perspectives on endothelial-to-mesenchymal transition: potential contribution to vascular remodeling in chronic pulmonary hypertension.* Am J Physiol Lung Cell Mol Physiol, 2007. **293**(1): p. L1-8.

13. Sumual S, Saad S, Tang O, Yong R, McGinn S, Chen XM, and Pollock CA. *Differential regulation of Snail by hypoxia and hyperglycemia in human proximal tubule cells.* Int J Biochem Cell Biol, 2010. **42**(10): p. 1689-97.

14. Zeisberg M and Neilson EG. *Biomarkers for epithelial-mesenchymal transitions.* J Clin Invest, 2009. **119**(6): p. 1429-37.

15. Zeisberg EM, Tarnavski O, Zeisberg M, Dorfman AL, McMullen JR, Gustafsson E, Chandraker A, Yuan X, Pu WT, Roberts AB, Neilson EG, Sayegh MH, Izumo S, and Kalluri R. *Endothelial-to-mesenchymal transition contributes to cardiac fibrosis.* Nat Med, 2007. **13**(8): p. 952-61.

16. Ghosh AK, Nagpal V, Covington JW, Michaels MA, and Vaughan DE. *Molecular basis of cardiac endothelial-to-mesenchymal transition (EndMT): differential expression of microRNAs during EndMT.* Cell Signal, 2012. **24**(5): p. 1031-6.

17. Eisenberg LM, and Markwald RR. *Molecular regulation of atrioventricular valvuloseptal morphogenesis.* Circ Res, 1995. **77**(1): p. 1-6.

18. Kuwahara F, Kai H, Tokuda K, Kai M, Takeshita A, Egashira K, and Imaizumi T. *Transforming growth factor-beta function blocking prevents myocardial fibrosis and diastolic dysfunction in pressure-overloaded rats.* Circulation, 2002. **106**(1): p. 130-5.

19. Upton PD, and Morrell NW. *TGF-beta and BMPR-II pharmacology--implications for pulmonary vascular diseases.* Curr Opin Pharmacol, 2009. **9**(3): p. 274-80.

20. Reynolds AM, Holmes MD, Danilov SM, Reynolds PN. *Targeted gene delivery of BMPR2 attenuates pulmonary hypertension.* Eur Respir J, 2012. **39**(2): p. 329-43.

21. Li S, Li H, MingyanE, and Yu B. *Expression of TGFbeta1 in pulmonary vein stenosis after radiofrequency ablation in chronic atrial fibrillation of dogs.* Mol Biol Rep, 2009. **36**(2): p. 221-5.

22. Richter B, Gwechenberger M, Socas A, Zom G, Albinni S, Marx M,Wolf F, Bergler-Klein J, Loewe C, Biegilmayer C, Binder T, Wojta J, and Gössinger HD. *Time course of markers of tissue repair after ablation of atrial fibrillation and their relation to left atrial structural changes and clinical ablation outcome.* Int J Cardiol, 2011. **152**(2): p. 231-6.

23. LaBourene JI, Coles JG, Johnson DJ, Mehra A, Keeley FW, and Rabinovitch M. *Alterations in elastin and collagen related to the mechanism of progressive pulmonary venous obstruction in a piglet model. A hemodynamic, ultrastructural, and biochemical study.* Circ Res, 1990. **66**(2): p. 438-56.

24. Schwartz RS, Huber KC, Murphy JG, Edwards WD, Camrud AR, Vlietstra RE, and Holmes DR. *Restenosis and the proportional neointimal response to coronary artery injury: results in a porcine model.* J Am Coll Cardiol, 1992. **19**(2): p. 267-74.

25. Suzuki T, Kopia G, Hayashi S, Bailey LR, Llanos G, Wilensky R, Klugherz BD, Papandreou G, Narayan P, Leon MB, Yeung AC, Tio F, Tsao PS, Falotico R, and Carter AJ. *Stent-Based Delivery of Sirolimus Reduces Neointimal Formation in a Porcine Coronary Model.* Circulation, 2001. **104**(10): p. 1188-1193.

26. Furukawa T, Kishiro M, Fukunaga H, Ohtsuki M, Takahashi K, Akimoto K, Shimizu T, Kawasaki S, and Kumasaka T. *Drug-Eluting Stents Ameliorate Pulmonary Vein Stenotic Changes in Pigs In Vivo.* Pediatric Cardiology, 2010. **31**(6): p. 773-779.

27. Unverferth DV, Baker PB, Swift SE, Chaffee R, Fetters JK, Uretsky BF, Thompson ME, and Leier CV. *Extent of myocardial fibrosis and cellular hypertrophy in dilated cardiomyopathy.* Am J Cardiol, 1986. **57**(10): p. 816-20.

28. Masszi A, and Kapus A. *Smaddening complexity: the role of Smad3 in epithelial-myofibroblast transition.* Cells Tissues Organs, 2011. **193**(1-2): p. 41-52.

29. Chapman HA. *Epithelial-mesenchymal interactions in pulmonary fibrosis.* Annu Rev Physiol, 2011. **73**: p. 413-35.

30. Boonla C, Krieglstein K, Bovornpadungkitti S, Strutz F, Spittau B, Predanon C, and Tosukhowong P. *Fibrosis and evidence for epithelial-mesenchymal transition in the kidneys of patients with staghorn calculi.* BJU Int, 2011. **108**(8): p. 1336-45.

31. Vongwiwatana A, Tasanarong A, Rayner DC, Melk A, and Halloran PF. *Epithelial to mesenchymal transition during late deterioration of human kidney transplants: the role of tubular cells in fibrogenesis.* Am J Transplant, 2005. **5**(6): p. 1367-74.

32. Kitao A, Sato Y, Sawada-Kitamura S, Harada K, Sasaki M, Morikawa H, Shiomi S, Honda M, Matsui O, and Nakanuma Y. *Endothelial to mesenchymal transition via transforming growth factor-beta1/Smad activation is associated with portal venous stenosis in idiopathic portal hypertension.* Am J Pathol, 2009. **175**(2): p. 616-26.

33. Hashimoto N, Phan SH, Imaizumi K, Matsuo M, Nakashima H, Kawabe T, Shimokata K, and Hasegawa Y. *Endothelial-mesenchymal transition in bleomycin-induced pulmonary fibrosis.* Am J Respir Cell Mol Biol, 2010. **43**(2): p. 161-72.

34. Maleszewska M, Moonen JR, Huijkman N, van de Sluis B, Krenning G, and Harmsen MC. *IL-1beta and TGFbeta2 synergistically induce endothelial to mesenchymal transition in an NFkappaB-dependent manner.* Immunobiology, 2013. **218**(4): p. 443-54.

35. Mihira H, Suzuki HI, Akatsu Y, Yoshimatsu Y, Igarashi T, Miyazono K, and Watabe T. *TGF-beta-induced mesenchymal transition of MS-1 endothelial cells requires Smad-dependent cooperative activation of Rho signals and MRTF-A.* J Biochem, 2012. **151**(2): p. 145-56.

36. van Meeteren LA, and ten Dijke P. *Regulation of endothelial cell plasticity by TGF-beta.* Cell Tissue Res, 2012. **347**(1): p. 177-86.

37. Medici D, Potenta S, and Kalluri R. *Transforming growth factor-beta2 promotes Snail-mediated endothelial-mesenchymal transition through convergence of Smad-dependent and Smad-independent signalling.* Biochem J, 2011. **437**(3): p. 515-20.

38. Yuen CY, Wong SL, Lau CW, Tsang SY, Xu A, Zhu Z, Ng CF, Yao X, Kong SK, Lee HK, and Huang Y. *From skeleton to cytoskeleton: osteocalcin transforms*

vascular fibroblasts to myofibroblasts via angiotensin II and Toll-like receptor 4. Circ Res, 2012. **111**(3): p. e55-66.

39. Yeager ME, Frid MG, and Stenmark KR. *Progenitor cells in pulmonary vascular remodeling.* Pulm Circ, 2011. **1**(1): p. 3-16.

40. Darby I, Skalli O, and Gabbiani G. *Alpha-smooth muscle actin is transiently expressed by myofibroblasts during experimental wound healing.* Lab Invest, 1990. **63**(1): p. 21-9.

41. Sarrazy V, Billet F, Micallef L, Coulomb B, and Desmoulière A. *Mechanisms of pathological scarring: role of myofibroblasts and current developments.* Wound Repair Regen, 2011. **19 Suppl 1**: p. s10-5.

42. Shi ZD, Ji XY, Qazi H, and Tarbell JM. *Interstitial flow promotes vascular fibroblast, myofibroblast, and smooth muscle cell motility in 3-D collagen I via upregulation of MMP-1.* Am J Physiol Heart Circ Physiol, 2009. **297**(4): p. H1225-34.

43. MacLeod DC, Strauss BH, de Jong M, Escaned J, Umans VA, van Suylen RJ, Verkerk A, de Feyter PJ, and Serruys PW. *Proliferation and extracellular matrix synthesis of smooth muscle cells cultured from human coronary atherosclerotic and restenotic lesions.* J Am Coll Cardiol, 1994. **23**(1): p. 59-65.

44. Weber KT. *Monitoring tissue repair and fibrosis from a distance.* Circulation, 1997. **96**(8): p. 2488-92.

45. Keeley EC, Mehrad B, and Strieter RM. *Fibrocytes: bringing new insights into mechanisms of inflammation and fibrosis.* Int J Biochem Cell Biol, 2010. **42**(4): p. 535-42.

46. Frid MG, Brunetti JA, Burke DL, Carpenter TC, Davie NJ, Reeves JT, Roedersheimer MT, van Rooijen N, and Stenmark KR. *Hypoxia-induced pulmonary vascular*

remodeling requires recruitment of circulating mesenchymal precursors of a monocyte/macrophage lineage. Am J Pathol, 2006. **168**(2): p. 659-69.

47. Yue WM, Liu W, Bi YW, He XP, Sun WY, Pang XY, Gu XH, and Wang XP. *Mesenchymal stem cells differentiate into an endothelial phenotype, reduce neointimal formation, and enhance endothelial function in a rat vein grafting model.* Stem Cells Dev, 2008. **17**(4): p. 785-93.

48. Diez M, Musri MM, Ferrer E, Barberà JA, and Peinado VI. *Endothelial progenitor cells undergo an endothelial-to-mesenchymal transition-like process mediated by TGFbetaRI.* Cardiovasc Res, 2010. **88**(3): p. 502-11.

49. Tanaka K, Sata M, Hirata Y, and Nagai R. *Diverse contribution of bone marrow cells to neointimal hyperplasia after mechanical vascular injuries.* Circ Res, 2003. **93**(8): p. 783-90.

[Figure legends]

Figure 1: Scheme of hypothesis for PV fibrosis

PV endothelial injury triggers TGF-β mediated EndMT and consequently myofibroblast proliferation leads to upstream PV fibrosis.

Figure 2: Histology and immunofluorescence staining in human and piglet pulmonary veins

A: human pulmonary vein histology from a PVS patient; Movat pentachrome staining showed fibromuscular hyperplasia. B: human PVS lung tissue; elastic trichrome staining demonstrated marked pulmonary vein intimal hyperplasia (arterialization) with luminal narrowing. C-G: Pulmonary veins from a TAPVD patient with PVS. (400× magnification) Compared with the control histology; H-L: control pulmonary veins from a heart transplant donor without PVS, endothelial markers (CD 31 and vWF: D, E) were decreased and expression of TGF-β1 (C) and mesenchymal markers (fibronectin and α-SMA; F, G) were increased in the TAPVD patient, consistent with the piglet study. M-P: HE staining of upstream pulmonary veins in the piglet model. M-N: sham group; O-P: banded group. Banded PVs had increased intimal thickness (red arrows in P). intimal thickness as percentage of intimal + medial layer thickness was greater in banded pulmonary veins. *: $p < 0.05$ Q-R: representative microvascular changes in the lung. Q: lung tissue in the sham group had thin walled pulmonary veins. R: lung tissue in the banded group had intimal hyperplasia in pulmonary veins. TAPVD: total anomalous pulmonary venous drainage; vWF: Von Willebrand factor; α-SMA: alpha smooth muscle actin.

Figure 3: RV myocyte fiber size and collagen deposition

Left panels; HE staining of RV muscle. Black arrows showed myocyte fiber thickness. Right panels; Trichrome staining of RV muscles. Banded group had thicker RV myocyte fiber size and much more collagen deposition (blue stained) in RV tissue.

Figure 4: Representative gain of mesenchymal and decrease of endothelial markers in immunofluorescent staining of upstream pulmonary veins of the piglet PVS model

A-C, G-I: upstream pulmonary veins in the sham group; D-F, J-L: upstream pulmonary veins in the banded group; Banded pulmonary veins exhibited greater expression of mesenchymal markers (fibronectin, FSP-1, and α-SMA, A-F: 400× magnification) and less expression of endothelial markers (CD31, vWF and VE-cadherin, G-L: 400× magnification) compared to sham pulmonary veins. The banded upstream PV demonstrated increased expression of α-SMA and decreased expression of CD31 and VE-cadherin in Western-blot analysis. *: $p < 0.05$ FSP-1: fibroblast specific protein 1, α-SMA: alpha smooth muscle actin, VE-cad: vascular endothelial cadherin.

Figure 5: Co-expression of endothelial and mesenchymal markers confirming the presence of the EndMT transitional cell phenotype

A-C, H: upstream pulmonary veins in the sham group; D-G, I; upstream pulmonary veins in the banded group; A-F: Immunofluorescence showed decreased endothelial and increased mesenchymal markers in banded PVs; G: In the banded group, intimal cells expressed an endothelial marker (CD31 in red) in the outer membrane and a mesenchymal marker (α-SMA in green) in the intracellular space, consistent with a EndMT transitional cell. (600× magnification); H-I: expression of TGF-β1; Banded pulmonary veins demonstrated greater expression of TGF-β1

compared to sham pulmonary veins (400× magnification). Western-blot analysis supported increased expression of TGF-β1 and Smad 4 in banded upstream PVs ($p = 0.01$ and $p = 0.049$ respectively). S; Sham, B; Banded.

Figure 6: Representative immunofluorescent staining and HE staining of stented piglet PVs

A-E: upstream pulmonary veins in the stented group. F-J: upstream pulmonary veins in the banded group. Upstream pulmonary veins from stented piglets demonstrated moderately increased TGF-β1 expression, regained endothelial markers (B, C) and strong expression of mesenchymal markers (D, E). K: representative HE staining of a pulmonary veins with stent from a stented piglet demonstrated in-stent re-stenosis. Arrow indicates stent fragments inside the pulmonary venous wall. (50× magnification) A graph on the right shows the percentage of in-stent restenosis 4 weeks post-stenting in each stent area. Average area percentage of in-stent stenosis was 43.46 ± 27.85 %.

Figure 7: Induction of EndMT *in vitro*

High content imaging of cultured piglet pulmonary vein cells and HUVECs.

A, C; control banded piglet PV cells. B, D; banded piglet PV cells treated with TGF-β1 (5 ng/ml, 48 hours). E, G; control HUVECs. F, H; HUVECs treated with TGF-β1 (5 ng/ml, 48 hours). The cells treated with TGF-β1 showed an increase in the myofibroblast markers; fibronectin and α-SMA capturing the EndMT transitional process ($p < 0.05$ versus control).

[Figures]

Figure 1: Scheme of hypothesis for PV fibrosis

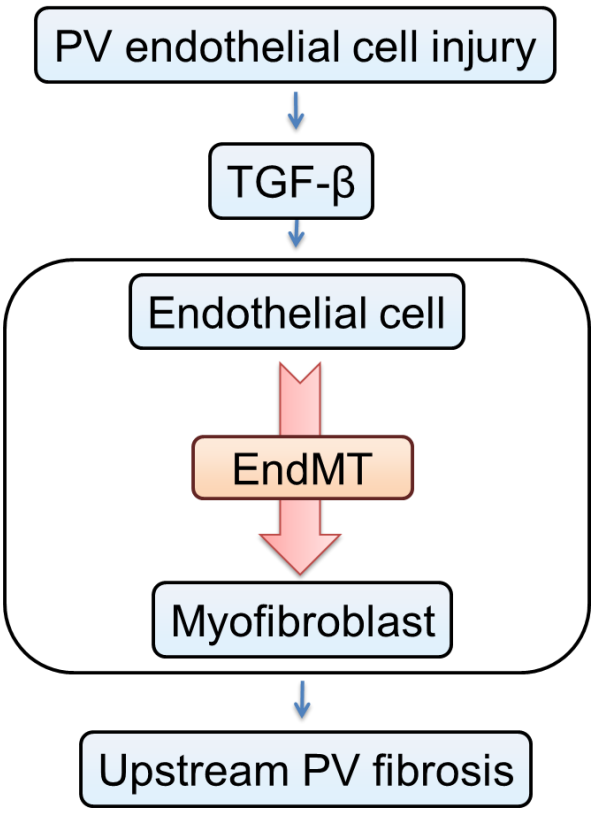

Figure 2: Histology and immunofluorescence staining in human and piglet pulmonary veins

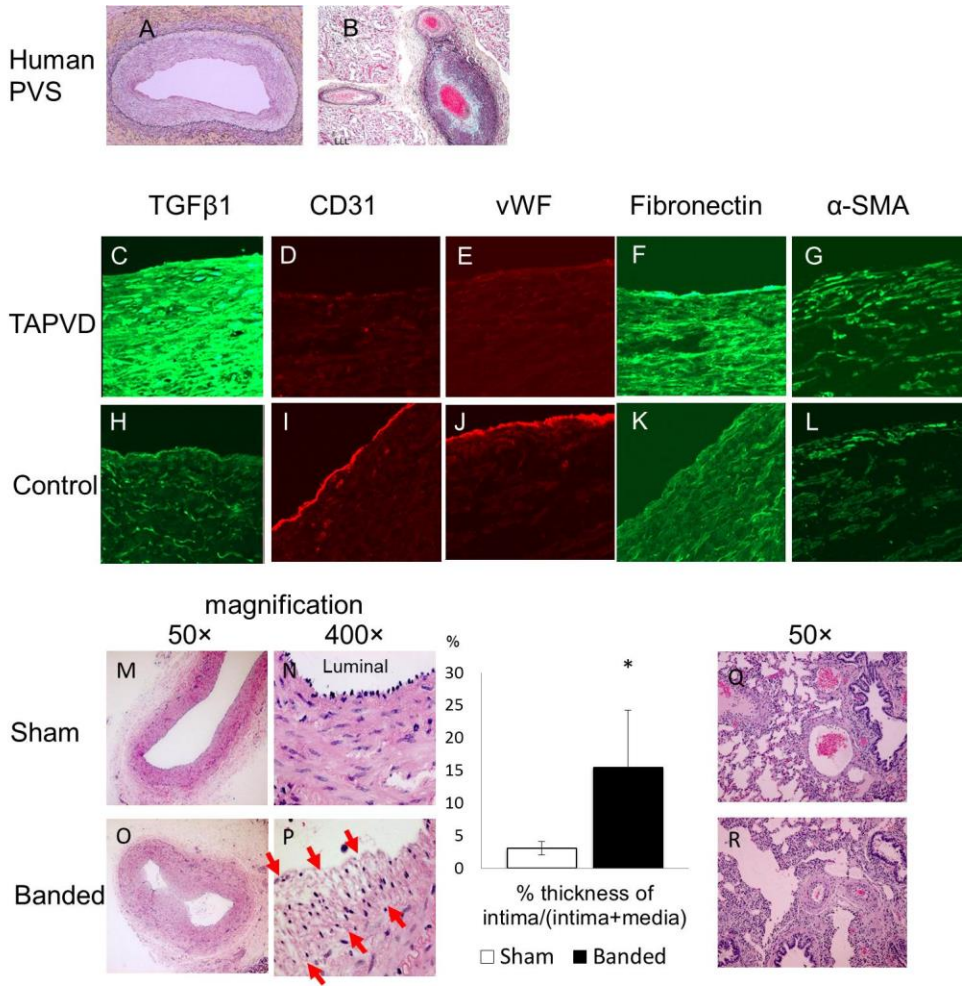

Figure 3: RV myocyte fiber size and collagen deposition

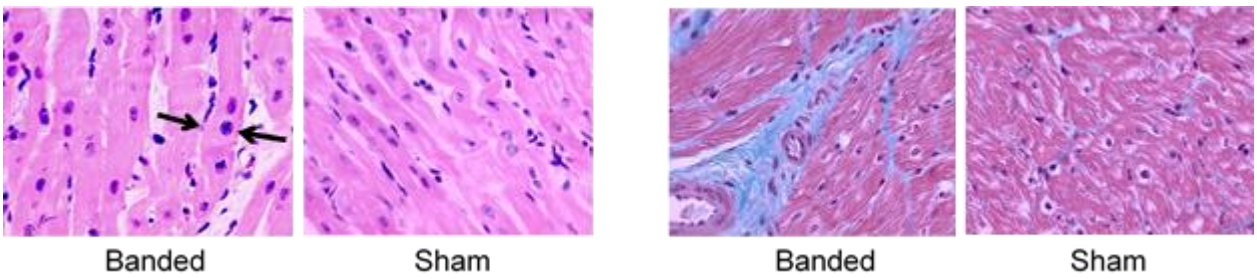

Figure 4: Representative gain of mesenchymal and decrease of endothelial markers in immunofluorescent staining of upstream pulmonary veins of the piglet PVS model

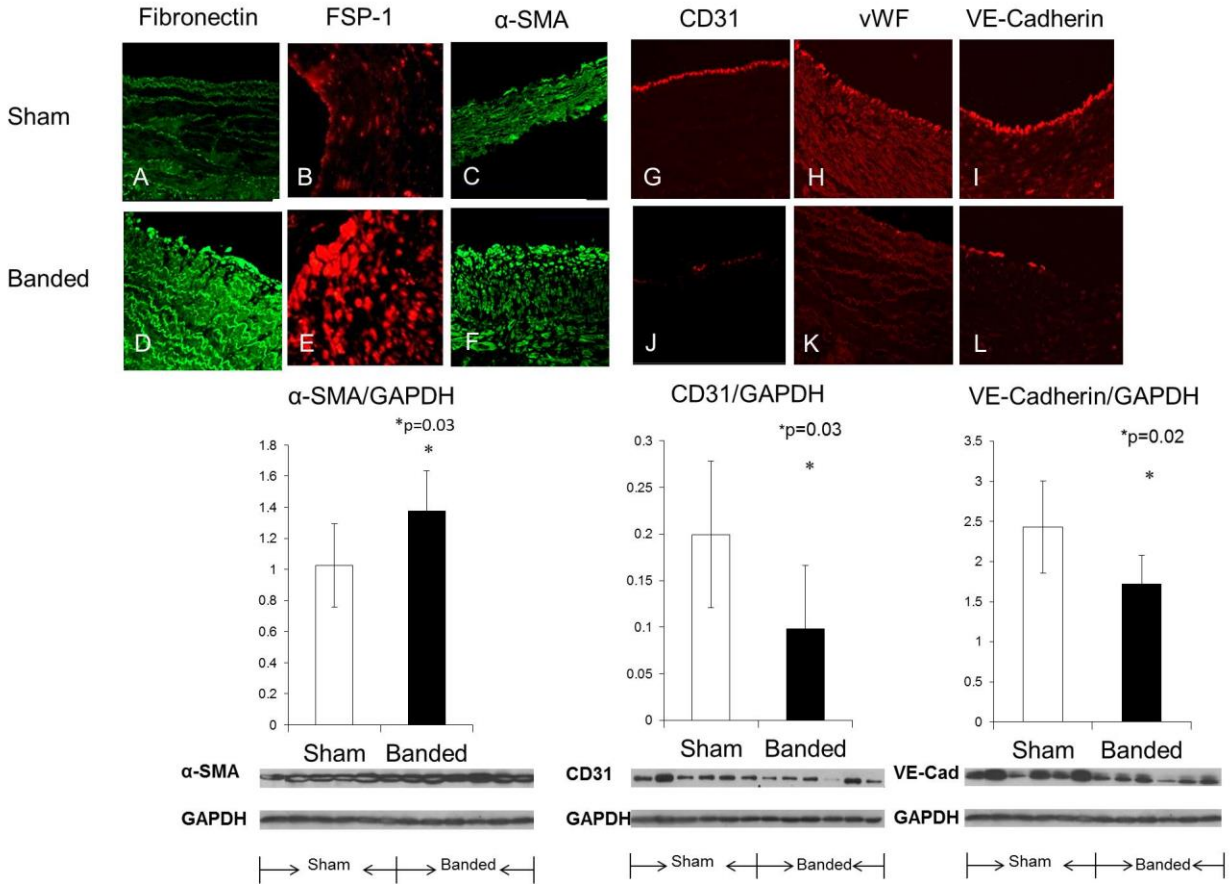

Figure 5: Co-expression of endothelial and mesenchymal markers confirming the presence of the EndMT transitional cell phenotype

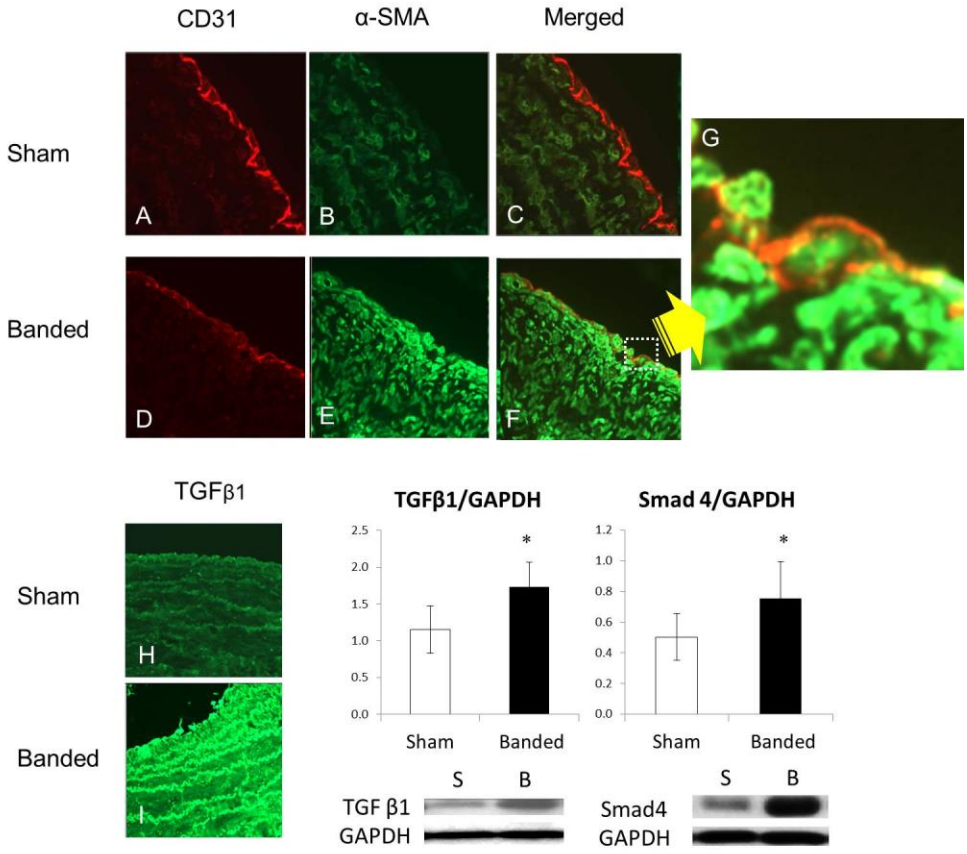

Figure 6: Representative immunofluorescent staining and HE staining of stented piglet PVs

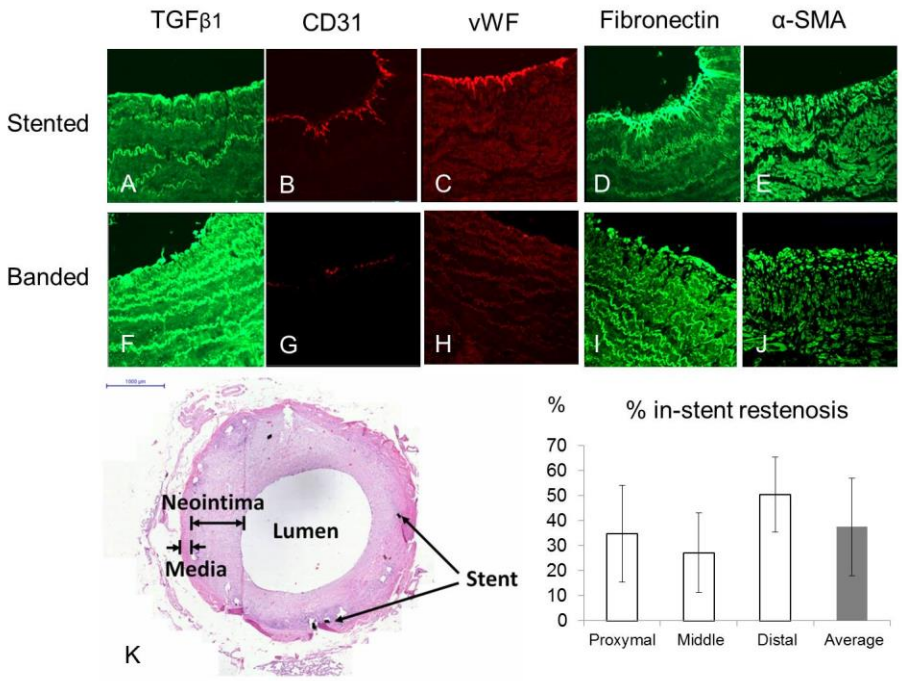

Figure 7: Induction of EndMT *in vitro*

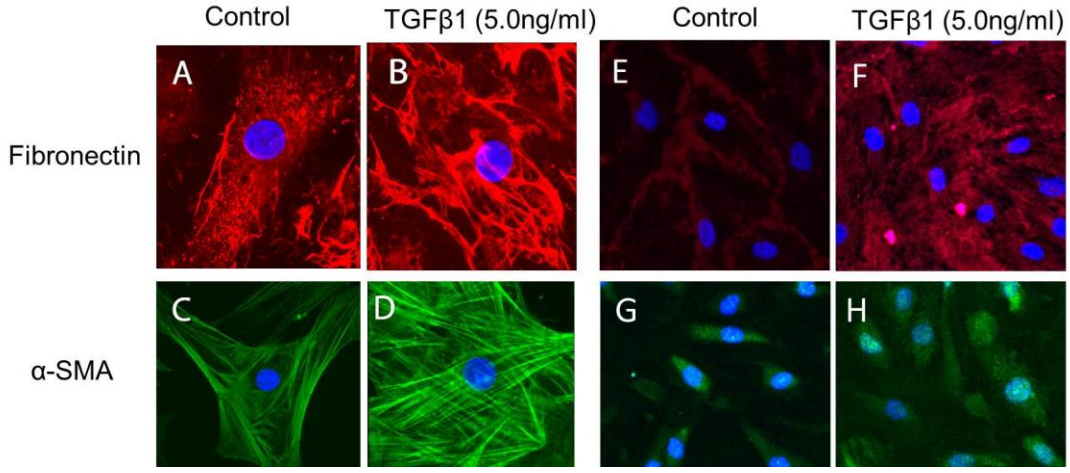

[Tables]

Table 1: Echocardiographic data

	3 weeks post-procedure			6 weeks post-procedure		
	Banded(n=6)	Sham(n=6)	p-value	Banded(n=6)	Sham(n=6)	p-value
HR (/min)	148.7±17.9	132.3±11.3	0.09	125.5±21.2	116.7±5.75	0.36
PVG (mmHg)	6.67±3.14	2.00±1.10	*0.01	11.50±4.76	1.20±0.45	*0.009
RVSP (mmHg)	38.83±11.23	27.25±5.25	0.06	52.17±18.03	23.25±3.30	*0.01
RVEDD (cm)	1.53±0.20	1.59±0.35	0.74	2.23±0.52	1.90±0.45	0.30
IVSD (cm)	0.67±0.13	0.62±0.06	0.60	0.73±0.09	0.76±0.06	0.68
LVEDD (cm)	3.31±0.52	3.50±0.28	0.53	3.81±0.54	4.10±0.46	0.37
LVSF (%)	34.50±4.43	33.69±3.06	0.72	38.20±6.05	36.3±4.45	0.58

HR: heart rate, PVG: pulmonary vein gradient, RVSP: right ventricular systolic pressure, RVEDD: right ventricular end-diastolic dimension, IVSD: interventricular septal width at diastole, LVEDD: left right ventricular end-diastolic dimension, LVSF: left ventricular shortening fraction.

Table 2: Hemodynamic data

Hemodynamics at 7 weeks post procedure					
	Banded(n=6)	Sham(n=6)	Stent(n=6)	[x]p-value	[$]p-value
BW (kg)	27.2±7.07	29.7±2.90	22.4±3.94	0.46	0.19
HR (bpm)	127.2±45.54	99.8±10.94	120.7±22.38	0.21	0.76
BSA (cm2)	6864.8±800.8	7444.5±217.8	6463.7±433.2	0.40	0.19
ABP systolic (mmHg)	67.17±6.08	70.50±7.92	68.67±9.0	0.43	0.74
CVP (mmHg)	4.33±4.08	1.83±1.48	5.50±2.88	0.21	0.58
RVP systolic (mmHg)	38.83±8.77	19.50±2.43	44.67±9.69	<0.01	0.30
RVP/ABP	0.64±0.12	0.28±0.02	0.66±0.14	<0.01	0.44
PAP systolic (mmHg)	39.83±9.20	16.17±2.14	44.67±8.59	<0.01	0.37
PAP/ABP	0.65±0.18	0.23±0.02	0.79±0.15	<0.01	0.17
PCWP (mmHg)	11.33±3.08	5.33±2.34	14.67±3.67	<0.01	0.12
CO (L/min)	3.61±0.62	4.55±0.67	3.18±0.90	0.03	0.35
CI (L/min/kg)	0.14±0.02	0.15±0.02	0.14±0.03	0.26	0.78
PVR (mmHg*min/L)	7.54±2.92	1.44±0.25	7.64±2.60	0.01	0.61
SVR (mmHg*min/L)	13.67±2.03	11.16±2.57	13.69±1.45	0.07	0.93
Comp (ml/mmHg)	1.81±1.34	7.20±1.58	1.26±0.53	<0.01	0.38
RVEDP (mmHg)	4.33±2.07	2.50±1.64	4.80±0.53	0.12	0.75
LVEDP (mmHg)	3.67±2.07	2.67±2.34	5.60±3.36	0.45	0.30
RVP/LVP	0.64±0.18	0.33±0.04	0.74±.014	<0.01	0.28
RV weight (g)	51.2±15.1	33.9±1.18	48.4±14.2	0.04	0.75
RV/LV+S	0.65±0.10	0.35±0.02	0.73±.015	0.01	0.17

BW; body weight, HR; heart rate, BSA; body surface area, ABP; arterial blood pressure, CVP; central venous pressure, RVP; right ventricular pressure, PAP; pulmonary arterial pressure, PCWP; pulmonary capillary wedge pressure, CO; cardiac output, CI; cardiac index, PVR; pulmonary vascular resistance, SVR: systemic vascular resistance, Comp; pulmonary vascular compliance, RVEDP; right ventricular end-diastolic pressure, LVEDP; left ventricular end-diastolic pressure, RV/LV+S; ratio of weight of right ventricle against left ventricular and septal weight * p-value in comparison between banded and sham groups ʿ p-value in a comparison between banded and stent groups